Nucleophilic Degradation of Fenitrothion Insecticide and Performance of Nucleophiles: A Computational Study

ARTICLE *in* THE JOURNAL OF PHYSICAL CHEMISTRY A · MARCH 2012

Impact Factor: 2.69 · DOI: 10.1021/jp2100057 · Source: PubMed

3 AUTHORS, INCLUDING:

Debasish Mandal
Hebrew University of Jerusalem
29 PUBLICATIONS **153** CITATIONS
SEE PROFILE

Bhaskar Mondal
Max Planck Institute for Chemical Energy Con…
30 PUBLICATIONS **121** CITATIONS
SEE PROFILE

THE JOURNAL OF PHYSICAL CHEMISTRY A

Article

pubs.acs.org/JPCA

Nucleophilic Degradation of Fenitrothion Insecticide and Performance of Nucleophiles: A Computational Study

Debasish Mandal, Bhaskar Mondal,[†] and Abhijit K. Das*

Department of Spectroscopy, Indian Association for the Cultivation of Science, Jadavpur, Kolkata 700 032, India

Supporting Information

ABSTRACT: Ab initio and density functional theory (DFT) calculations have been performed to understand the destruction chemistry of an important organophosphorus insecticide *O*,*O*-dimethyl *O*-(3-methyl-4-nitrophenyl) phosphorothioate, fenitrothion (**FN**), toward nucleophilic attack. Breaking of the P−OAr linkages through nucleophilic attack is considered to be the major degradation pathway for **FN**. One simple nucleophile, hydroxide (OH^-), and two different α-nucleophiles, hydroperoxide (OOH^-) and hydroxylamine anion (NH_2O^-), have been considered for this study. Nucleophilic attack at the two different centers, S_N2@P and S_N2@C, has been monitored, and the computed reaction energetics confirms that the S_N2@P reactions are favorable over the S_N2@C reactions for all the nucleophiles. All electronic structure calculations for the reaction are performed at DFT-B3LYP/6-31+G(d) level of theory followed by a refinement of energy at ab initio MP2/6-311++G(2d,2p) level. The effect of aqueous polarization on both the S_N2 reactions is taken into account employing the conductor-like screening model (COSMO) as well as polarization continuum model (PCM) at B3LYP/6-31+G(d) level of theory. Relative performance of the two α-nucleophiles, OOH^- and NH_2O^-, at the P center has further been clarified using natural bond orbital (NBO), conceptual DFT, and atoms in molecules (AIM) approaches. The strength of the intermolecular hydrogen bonding in the transition states and topological properties of the electron density distribution for −X−H···S (X = O, N) intermolecular hydrogen bonds are the subject of NBO and AIM analysis, respectively. Our calculated reaction energetics and electronic properties suggest that the relative order of nucleophilicity for the nucleophiles is OOH^- > NH_2O^- > OH^- for the S_N2@P, whereas for the S_N2@C the order, which gets little altered, is NH_2O^- > OOH^- > OH^-.

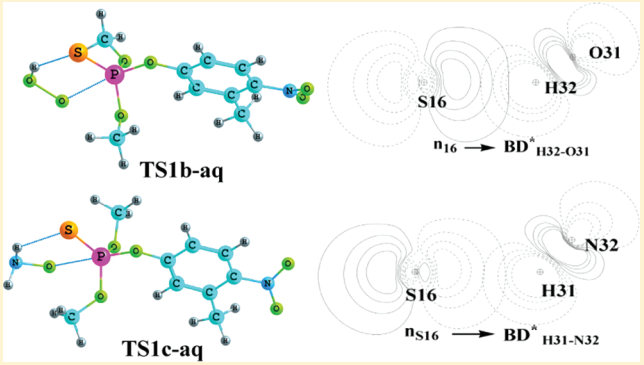

1. INTRODUCTION

Organophosphorus compounds (OPC) are extensively used in agriculture for field crop protection against insects. Their importance as pesticides for increasing the world's food production over the last few decades is well-recognized. In contrast OPCs possess serious environmental concerns because of their toxicity to human beings, since OPCs are known to inhibit the activity of acetyl cholinesterase (AChE), an important protein responsible for the hydrolysis of the neurotransmitter acetylcholine.[1−6] Due to such biological and environmental importance of these compounds, efficient remediation strategies are extremely necessary. Various studies have been performed for the analysis of the natural degradation of OPCs through different processes, e.g., hydrolysis,[7−9] oxidation,[10] photolysis,[11] biodegradation[12] as well as treatments with α-nucleophiles.[13,14] Some recent researches have highlighted the fact that α-nucleophiles played an effective role in the degradation process of the above type of toxic compounds.[15,16] A number of theoretical investigations were performed for the thermal unimolecular decomposition,[17] hydrolysis,[18,19] and α-nucleophilic destruction[20] of such deadly agents. Fenitrothion [*O*,*O*-dimethyl *O*-(3-methyl-4-4nitrophenyl) phosphorothioate] (**FN**) is a well-known insecticide used for protecting a wide range of crops.[21] **FN** is also classified as an antiacetyl cholinesterase neurotoxin, but it is remarkably less toxic to mammals than other organophosphorus insecticides such as parathion (*O*,*O*-diethyl *O*-(4-nitrophenyl) phosphorothioate) and paraoxon (diethyl 4-nitrophenyl phosphate), the reason for which it is used widely.[22] Hence, the detailed chemistry of **FN** is of prime importance for environmental toxicity. In general, **FN** degrades in different ways such as hydrolysis,[2,21] photolysis,[5] and microbial degradation.[3,4] It is also efficiently catalyzed by metal ions like Cu^{2+}, Hg^{2+}, and Ag^+ in their hydrolysis reaction.[23−28] Numerous experimental studies were performed for the nucleophilic destruction of **FN** in aqueous solution[15] and in the presence of cationic surfactant micellar medium.[13,29] The nucleophilic reaction of **FN** may proceed via three different routes (Scheme 1): (1)

Received: October 18, 2011
Revised: February 15, 2012
Published: February 16, 2012

Scheme 1. Possible Competitive Pathways for the Nucleophilic Degradation of Fenitrothion

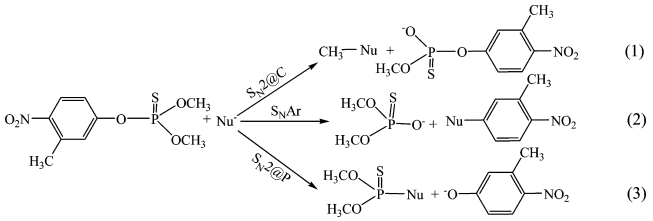

attack at the phosphorus center ($S_N2@P$), (2) attack at the aliphatic carbon of the methoxy group ($S_N2@C$), and (3) attack at the C-1 position of the aromatic ring (S_NAr).

The above possible pathways were detected with several nucleophiles in various experimental conditions.[13,15,29] Recently, Rougier et al.[15] performed an excellent study on **FN** with several simple and α-nucleophiles, e.g., hydroxide (OH^-), hydroperoxide (OOH^-), and hydroxylamine anion (NH_2O^-), etc., in basic aqueous solution. They observed that reaction at the P center was the only pathway observed with two O nucleophiles, OH^- and OOH^-, whereas competition with $S_N2@C$ was found with other nucleophiles, e.g., NH_2O^-, etc. No evidence of S_NAr was reported in any case, and it was also supported by another investigation.[13] This can be explained by the fact that in **FN** there is only one nitro group in the aromatic ring, and thus it is unlikely to be sufficiently electron deficient to favor an S_NAr reaction. It was established experimentally that α-nucleophiles were more effective destructive agents for **FN**. No theoretical studies can be found in the literature regarding nucleophilic reactions or other degradation procedures of **FN** with the exception of a molecular orbital description of the photolysis of **FN**[30] and two theoretical NMR studies of **FN**–Cu^{2+} and **FN**–Hg^{2+} for establishing the catalytic effect of Cu^{2+} and Hg^{2+} in the hydrolysis of **FN**.[31,32] In this report we present a systematic computational study of the solvolysis reaction of **FN** with simple (OH^-) and α-nucleophiles (OOH^- and NH_2O^-). The biological activity of molecules is known to be crucially dependent on the electronic structure of the active part of the given compound and its conformation. Thus, we initially performed a conformational analysis of **FN** using molecular dynamics (MD) and molecular mechanics (MM) approaches. We then proceed further and calculated electronic structure for the minimum energy conformer. As the $S_N2@P$ pathways are the major for **FN**, a detailed study of these pathways is discussed for the three nucleophiles. Furthermore, the Gibbs free energy (ΔG_{298k}) profile has also been constructed for the gas-phase and the aqueous-phase reactions. A comprehensive competitive study is performed to know the reactivity of the two α-nucleophiles, OOH^- and NH_2O^-, in the $S_N2@P$ reaction using the most common modern strategies, e.g., activation energy, conceptual density functional theory, natural bond orbital (NBO) analysis, and Bader's atoms in molecules (AIM) approach. The potential free energy profiles for the $S_N2@C$ reaction are built with free energies calculated in aqueous medium. The S_NAr pathways are beyond our calculation as they have no experimental evidence.

2. COMPUTATIONAL PROCEDURES

For computational investigation of conformational minima of **FN**, it is subjected to a molecular dynamics (MD) conformational search with an unconstrained MD trajectory via the Verlet velocity algorithm and NVE thermostat using other default parameters in Gabedit V.2.3.8.[33] The minimum conformational geometries are obtained using the PM6 semiempirical method as implemented in MOPAC 2009.[34] Additional molecular mechanics conformational studies are conducted using the MMFF94 force field and a systematic rotor search using Avogadro V.1.0.3.[35] For final validation of the conformational analysis, 25 representative minimum structures are selected from the rigorous conformational search and are treated with density functional theory. The geometries of all the molecular species involved in this study are fully optimized by employing density functional theory (DFT) using Becke's three-parameter hybrid exchange functional and the Lee–Yang–Parr correlation functional (B3LYP)[36−38] with the Pople's spilt-valence basis set 6-31+G(d) basis set.[39] Harmonic vibrational frequencies are determined at the same B3LYP/6-31+G(d) level to confirm whether the optimized structures are local minima (no imaginary frequency) or transition states (one imaginary frequency) on the potential energy surfaces (PESs) and to evaluate the zero-point vibrational energy (ZPVE) and thermal corrections to the Gibbs free energy at T = 298 K. The connecting first-order saddle points, that are the transition states between the equilibrium geometries, are obtained using the synchronous transit-guided quasi-Newton (STQN) method. A parallel intrinsic reaction coordinate (IRC) calculation is performed with all transition states to confirm whether these transition states connect the right minima or not.[40,41] To get more reliable energetics, single-point energy calculations are performed on the B3LYP/6-31+G(d) optimized geometries using the second-order Møller–Plesset perturbation theory (MP2)[42−45] with 6-311++G(2d,2p) basis set.

Two different self-consistent reaction field (SCRF) procedures have been employed to take into account the influence of water as a solvent and to analyze the reaction mechanism in the aqueous phase. The aqueous-phase calculations are carried out at the same level of theory similar to the gas-phase ones. The conductor-like screening solvation model (COSMO)[46] is used first to incorporate the solvent effect. All COSMO calculations in this study have been performed by using the default choice of the Gaussian 09 program[47] with the recommended standard parameters. To compare the reliability of the outcomes of the COSMO solvent model calculation, another SCRF procedure, the integral equation formalism polarized continuum solvation model (IEF-PCM) in water[48−52] is also employed for all of the above calculations. In the IEF-PCM computation, the united atom topological model (UA0)[50] radii is used in which no spheres are centered on the hydrogen; instead they are included inside the sphere centered on the heavy atom with which they are attached. The dielectric constant of water used for all of the solvation calculations is 78.35 D. The IEF-PCM model is also reliable and had been used in various typical investigations.[53] In comparison with experimental findings, it is found that the COSMO model provides more appropriate information on energetics than PCM. Therefore, we have used the aqueous-phase energetics as well as geometric parameters of the COSMO model in successive discussions, unless otherwise mentioned.

An AIM[54−56] analysis is performed to evaluate the strength of the intermolecular hydrogen bonding for transition state structure. For determination of the strength of the H-bond, the important topological parameters, electron density (ρBCP) and its Laplacian $\nabla^2\rho$BCP at the bond critical point (BCP), are calculated using the AIM 2000 program.[57]

dx.doi.org/10.1021/jp2100057 | J. Phys. Chem. A 2012, 116, 2536–2546

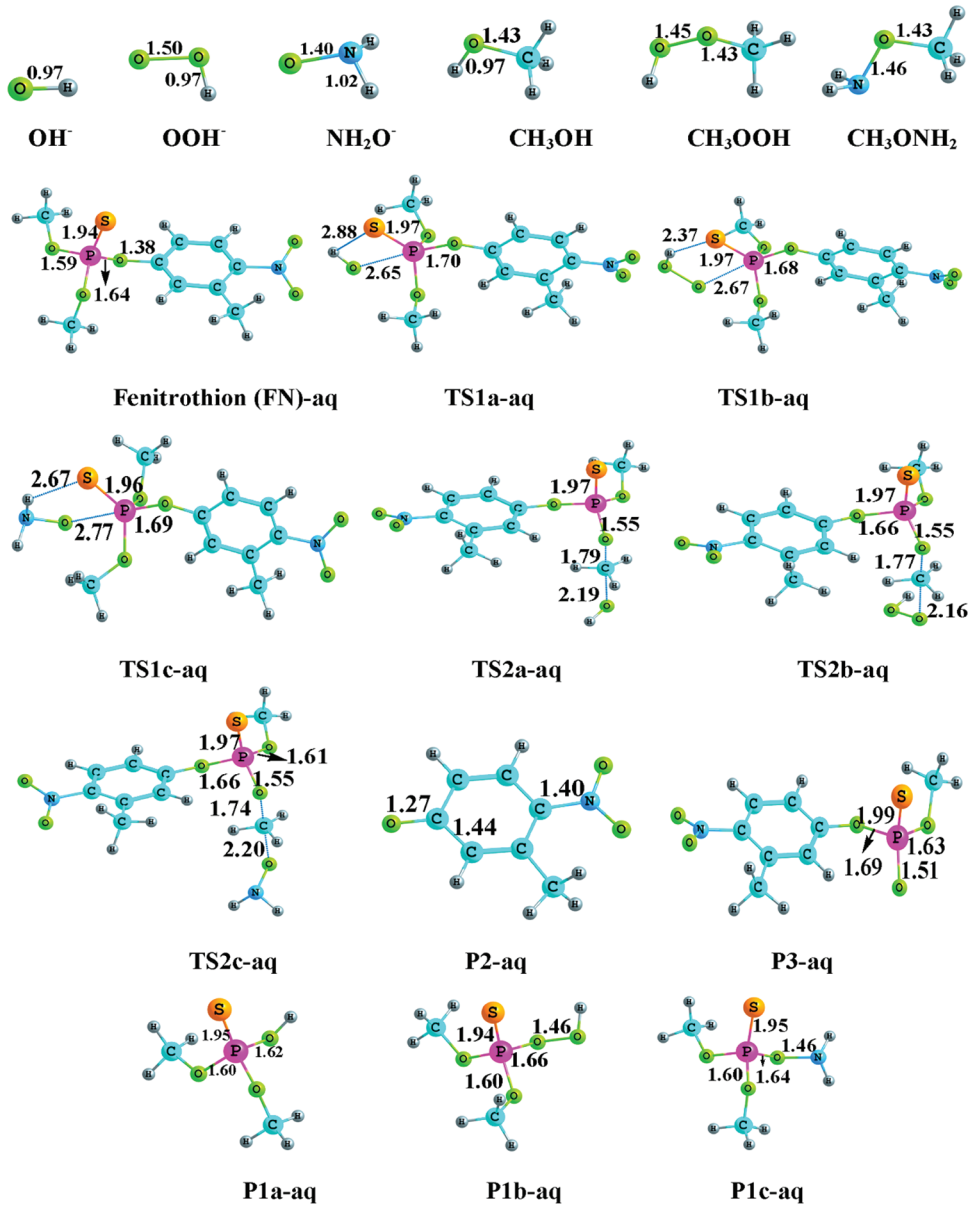

Figure 1. B3LYP/6-31+G(d) optimized geometries with important parameters in the aqueous phase for all the species involved in the reaction of fenitrothion with nucleophiles.

An NBO analysis is carried out for the evaluation of the bond order in transition state geometry. The NBO population analysis and Wiberg bond index calculation are performed using the NBO 3.1 program[58] as implemented in Gaussian 09.

The reactivity descriptor used in this work is related to the local softness, $s(r)$, by the following relation

$$s(r) = f(r)S$$

where S is the global softness of the system[59] and $f(r)$ is the Fukui function.[60] The condensed form of Fukui functions of an atom k in a molecule with N electrons is calculated using the finite difference approximation proposed by Yang and Mortier:[61]

$$f_k^+ = [q_k(N+1) - q_k(N)] \quad \text{for nucleophilic attack}$$

$$f_k^- = [q_k(N) - q_k(N-1)] \quad \text{for electrophilic attack}$$

The $q_k(N)$, $q_k(N-1)$, and $q_k(N+1)$ are the electron population for the atom k in the neutral, cationic, and anionic states of a system, respectively. These electron populations are evaluated at the neutral molecular geometry in both gas and aqueous phases. To compute f_k, we consider NPA,[62] Mulliken,[63] as well as Chelpg[64] charges calculated using the geometries optimized at B3LYP/6-31+G(d) level of theory.

The global softness (S) is computed from the finite difference formula

$$S = 1/(\mathrm{IE} - \mathrm{EA})$$

where IE and EA are the first vertical ionization energy and electron affinity, respectively. Koopman's theorem[65] allows the calculation of IE and EA as the energy of the lowest unoccupied molecular orbital (LUMO) and the highest occupied molecular

dx.doi.org/10.1021/jp2100057 | J. Phys. Chem. A 2012, 116, 2536–2546

Table 1. Relative Energies (ΔE, kcal/mol) Calculated at MP2/6-311++G(2d,2p)//B3LYP/6-31+G(d) Level of Theory and ΔH and ΔG Calculated at B3LYP/6-31+G(d) Level of Theory for All the Species Involved in the Solvolysis Reaction of Fenitrothion in the Aqueous Phase

	ΔE		ΔH		ΔG	
species	COSMO	PCM	COSMO	PCM	COSMO	PCM
FN + OH^-	0.00	0.00	0.00	0.00	0.00	0.00
TS1a-aq	10.22	6.73	11.02	5.39	20.52	15.40
TS2a-aq	13.96	8.67	12.16	7.28	20.39	15.45
TS2a′-aq	14.60	9.56	12.91	8.11	21.39	16.15
P1a-aq + **P2-aq**	−20.58	−29.66	−32.48	−41.54	−34.29	−43.24
P3 + CH_3OH	−34.92	−43.46	−20.17	−47.66	−40.36	−42.75
FN + OOH^-	0.00	0.00	0.00	0.00	0.00	0.00
TS1b-aq	3.38	2.17	6.57	4.26	18.68	16.83
TS2b-aq	10.77	8.00	10.34	6.68	20.09	16.57
TS2b′-aq	11.49	8.82	11.08	7.56	21.34	17.59
P1b-aq + **P2-aq**	−12.19	−17.47	−20.39	−25.15	−21.03	−25.71
P3 + CH_3OOH	−36.49	−42.32	−19.35	−43.27	−37.05	−42.74
FN + NH_2O^-	0.00	0.00	0.00	0.00	0.00	0.00
TS1c-aq	4.82	2.28	7.42	3.99	19.68	16.10
TS2c-aq	9.41	5.40	9.07	6.45	19.14	16.92
TS2c′-aq	10.09	5.91	9.79	5.62	19.49	15.78
P1c-aq + **P2-aq**	−23.48	−29.23	−32.29	−37.67	−62.25	−37.80
P3 + CH_3ONH_2	−42.66	−49.12	−23.02	−50.88	−45.43	−50.67

orbital (HOMO), respectively. So S can be obtained by the expression

$$S = 1/(E_{LUMO} - E_{HOMO})$$

Now the local softness of nucleophile and electrophile can be defined as

$$s_k^- = Sf_k^-$$

$$s_k^+ = Sf_k^+$$

In our study, s^+ represents the local softness of the P atom in **FN** and s^- represents the local softness of the O atom in nucleophiles. Gazquez[66] and Nguyen et al.[67] proposed a local version of the well-known hard soft acid base (HSAB) principle, and after generalization by Ponti,[68] it appears that the interaction between reaction partners is favored when it occurs through minimal $\Delta s(r)$, where

$$\Delta s(r) = |s^+(r) - s^-(r)|$$

All electronic structure calculations are performed using the Gaussian 09 suite of quantum chemistry programs.

3. RESULTS AND DISCUSSION

The minima for 25 selected conformers of **FN** are finally optimized using B3LYP/6-31+G(d) method in the gas phase. After DFT optimization we get six lower-energy structures having large dissimilar spatial arrangement. The detailed geometries (Supporting Information Figure S1) and energies (Supporting Information Table S1) are presented in the Supporting Information. For a careful evaluation of the reaction pathways at the P and aliphatic C centers, all species involved (reactants, transition states, and products) are optimized at B3LYP/6-31+G(d) level of theory in the aqueous phase. The optimized geometries are shown in Figure 1.

The relative energies calculated at MP2/6-311++G(2d,2p)//B3LYP/6-31+G(d) level and relative free energies and enthalpies calculated at B3LYP/6-31+G(d) level are presented in Table 1.

In the present theoretical study, all reactions follow the S_N2 pattern and proceed through direct displacement mechanism involving only one step in which the expulsion of a leaving group occurs at the same time when the substituting nucleophiles enter, i.e., in the concerted and asynchronous way, which is in good agreement with the comparable single-step hydrolysis mechanism of parathion and paraoxon.[18]

3.1. S_N2@P Reactions. The calculation of reaction indices for nucleophilic attack to **FN** shows that the reaction at the P center is the most important as well as favorable pathway than other displacement reactions.[30] The accepted mechanism of the reaction involves nucleophilic attack on the P atom of **FN** followed by the release of *p*-nitrophenol through the S_N2-type direct displacement pathway. These reactions are analyzed in the gas phase and also in the aqueous phase. In the gas phase, the nucleophilic S_N2 reactions generate a double-well PES on which reaction proceeds through the following way: reactant (**R**) → reactant complex (**RC**) → transition state (**TS**) → product complex (**PC**) → product (**P**). But in the polarized aqueous medium it shows a different pattern from gas-phase calculation, because we could not find any reactant or product complex on the PES. This suggests that the separated reactant goes directly to the product through the transition state following a single-well PES: reactant (**R**) → transition state (**TS**) → product (**P**). In each of the reactions negative entropy of activation is observed. The negative entropy of activation is an indication of an associative transition state, as expected for the bimolecular process. Here, the enthalpy of activation is the dominant contributor to the free energy of activation. The free energy barriers are discussed below for energetics, unless otherwise stated.

3.1.1. Hydrolysis. Let us first concentrate on the gas-phase hydrolysis mechanism. The concerted asynchronous hydrolysis pathway in the gas phase is presented in Figure 2 (channel a).

dx.doi.org/10.1021/jp2100057 | J. Phys. Chem. A 2012, 116, 2536−2546

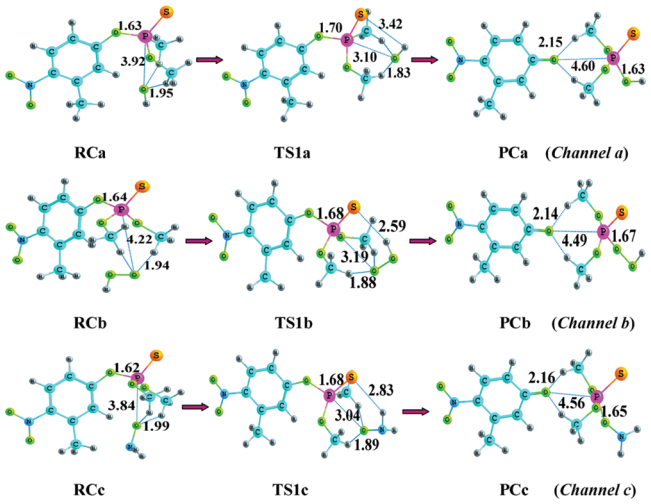

Figure 2. B3LYP/6-31+G(d) geometries for the stationary points along the reaction coordinate for the reaction of fenitrothion with simple (OH^-) and α-nucleophiles (HOO^- and NH_2O^-) in the gas phase.

The free energy profiles obtained from B3LYP/6-31+G(d) calculation for the hydrolysis of **FN** in the gas phase as well as in the aqueous phase are presented in Figure 3.

The coordinates of the gas-phase optimized geometries are given in the Supporting Information. In the gas phase, on arrival of the nucleophile a H-bonded reaction complex (**RCa**) is formed which is 29.07 kcal/mol lower in free energy with respect to the infinitely separated complex (**FN** + OH^-). In **RCa**, the P−OAr and P−OH distances are 1.63 and 3.92 Å, respectively. The **RCa** is stabilized through the formation of a hydrogen bond between the O of the nucleophile and H of the $-OCH_3$ moiety with a distance of 1.95 Å. Now nucleophilic attack occurs at the backside of the more potent leaving group, −OAr, through the transition state, **TS1a**, with activation energy (ΔE) of 10.12 and activation free energy of 6.52 kcal/mol. The activation energy is comparable with that obtained for the hydrolysis of paraoxon (7.40 kcal/mol) and parathion (8.60 kcal/mol).[18] The **TS1a** is an early transition state that has a triangular bipyramidal (TBP) geometry regarding the orientation of active atoms. In **TS1a**, the P−OAr distance is elongated by 0.07 Å and the P−OH distance is shortened by 0.82 Å. The **TS1a** then produces a product complex (**PCa**) through a highly exergonic pathway which is located 45.01 kcal/mol below the reactant complex, **RCa**, in the PES. In **PCa**, the P−OAr distance is elongated by 2.9 Å and the P−OH distance is shortened by 1.47 Å with respect to **TS1a**. This observation is corroborated with the complete breaking of the P−OAr bond in the product complex. It is also stabilized through the formation of the H-bond between the oxygen of −OAr and the hydrogen of $-OCH_3$. In the product complex, **PCa**, a complete inversion of stereochemistry at the phosphorus center is observed which clearly implies that the S_N2@P is a concerted process.

Figure 1 shows the geometric configuration of all the species optimized at B3LYP/6-31+G(d) level in the aqueous phase. For the reaction pathway studied in the aqueous phase, the infinitely separated reactants approach directly to the transition state, **TS1a-aq**, without forming any reactant complex. This may be due to the fact that in aqueous medium the ionic nucleophile gets more stabilized than hydrogen-bonded structures of the nucleophile with reactant in the gas phase. The **TS1a-aq** possesses free energy of activation and enthalpy of activation of 20.52 and 11.02 kcal/mol, respectively. The **TS1a-aq** has a very similar TBP geometry to those of **TS1a** and in **TS1a-aq**; the P−OH and P−OAr bond distances are 2.65 and 1.70 Å, respectively. The distance between the sulfur atom and the hydrogen of OH is 2.88 Å, which is significant for stabilization of the transition state. The product formation in the aqueous phase is calculated to be extremely exergonic (34.29 kcal/mol).

3.1.2. Hydroperoxidolysis. The reaction mechanism and energetics of **FN** with OOH^- is studied in both gas and in aqueous phases. The gas-phase optimized Cartesian coordinates are presented in the Supporting Information. The two-dimensional (2D) sketch of the relative free energy profile

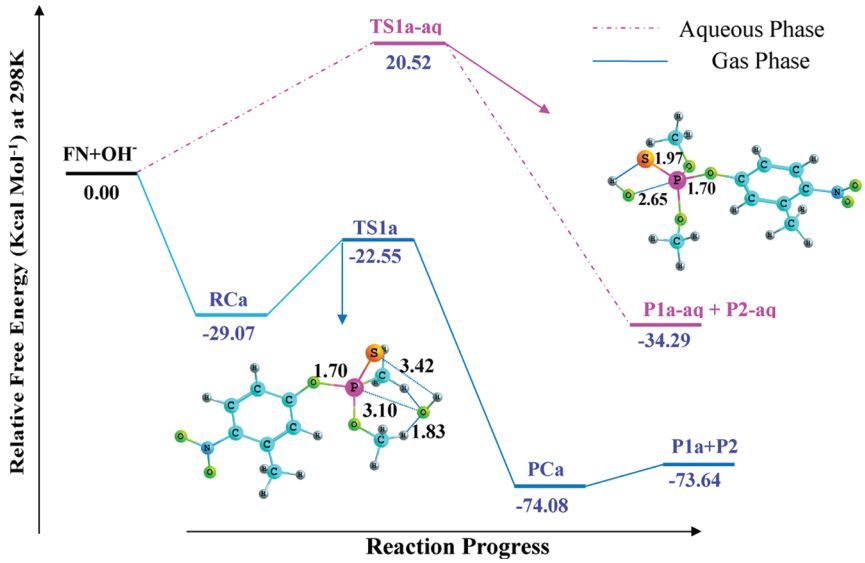

Figure 3. B3LYP/6-31+G(d) calculated free energy (ΔG_{298k}) profile for the reaction of fenitrothion with OH^- at the phosphorus center (S_N2@P) in gas and aqueous phases.

dx.doi.org/10.1021/jp2100057 | J. Phys. Chem. A 2012, 116, 2536−2546

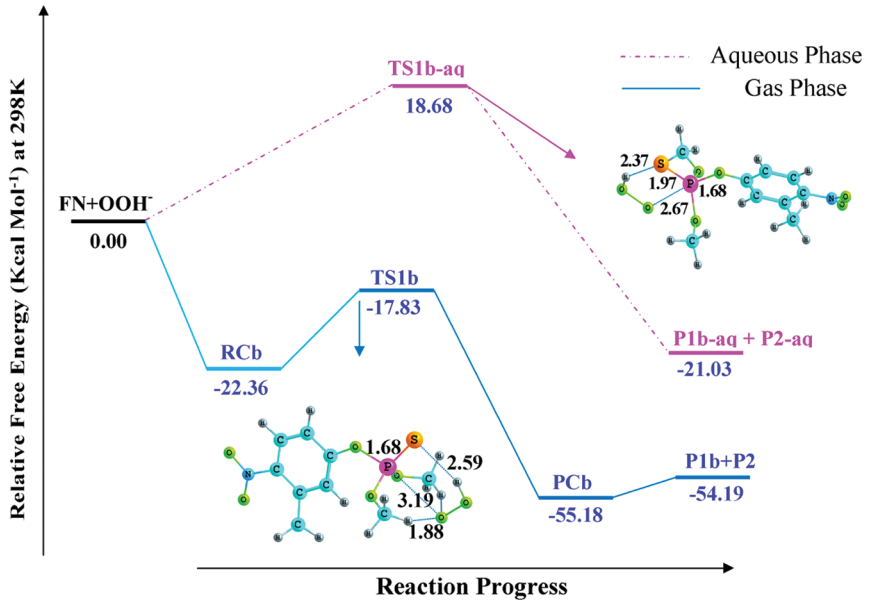

Figure 4. B3LYP/6-31+G(d) calculated free energy (ΔG_{298k}) profile for the reaction of fenitrothion with OOH^- at the phosphorus center (S_N2@P) in gas and aqueous phases.

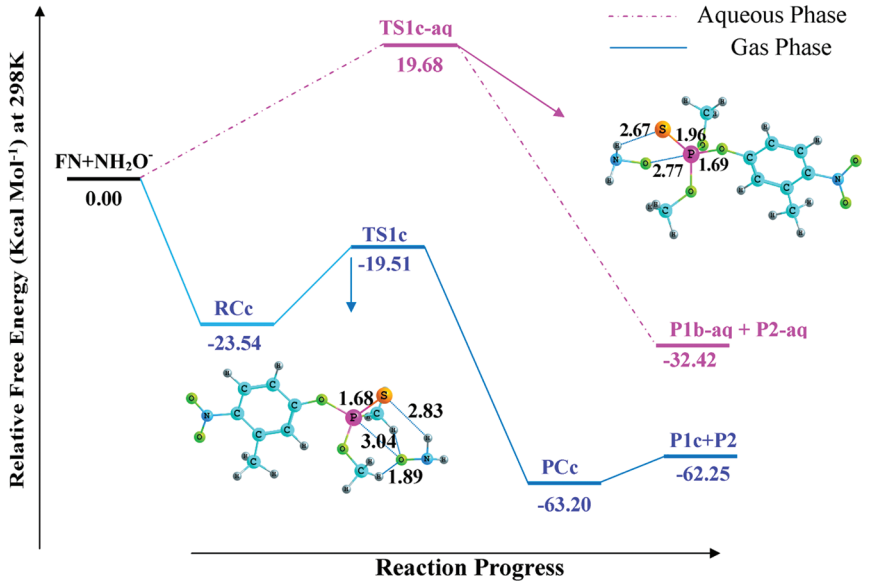

Figure 5. B3LYP/6-31+G(d) calculated free energy (ΔG_{298k}) profile for the reaction of fenitrothion with NH_2O^- at the phosphorus center (S_N2@P) in gas and aqueous phases.

(ΔG_{298k}) for the hydroperoxidolysis investigated in the gas as well as in the aqueous phase is presented in Figure 4.

The gas-phase reaction with hydroperoxide follows a similar mechanism as observed for the hydrolysis. A complete progress of the reaction described as channel b is presented in Figure 2. The reactants (**FN** and OOH^-) at first produce a weakly bonded reactant complex (**RCb**) which is located 22.36 kcal/mol below the infinitely separated reactants (**FN** + OOH^-). In case of **RCb**, the P−OAr and P−OOH distances are 1.64 and 4.22 Å, respectively. In **RCb**, the nucleophile, OOH^-, is oriented almost in a symmetric arrangement between the two $-OCH_3$ moieties of **FN**. The hydrogen bond between the oxygen of the nucleophile and the H of the $-OCH_3$ of **FN** has a interaction distance of 1.94 Å. The **RCb** then transforms further into a TBP geometric transition state, **TS1b**, having activation barrier 4.53 kcal/mol. The P−OAr and P−OOH detachments in **TS1b** have been increased and shortened by 0.03 and 1.03 Å, respectively, compared with that in **RCb**. Finally, **TS1b** transforms into the product complex, **PCb**, with symmetry inversion at the P center. In the free energy surface, **PCb** is located at 32.82 kcal/mol below the **RCb**. The active reaction parameters, P−OAr and P−OOH, change remarkably as it goes from **TS1b** to **PCb**. The P−OAr and P−OOH separations change from 1.67 to 4.49 and 3.19 to 1.67 Å, respectively.

The corresponding geometries for the hydroperoxidolysis of **FN** in the aqueous phase are given in Figure 1. Similar to the hydrolysis pathway explained above, the reaction of hydroperoxide in the aqueous phase goes without formation of a reactant complex and it proceeds through the transition state, **TS1b-aq**, which is the early TS that possesses the TBP geometry. The activation barrier for **TS1b-aq** is about 18.68

dx.doi.org/10.1021/jp2100057 | J. Phys. Chem. A 2012, 116, 2536−2546

Table 2. NBO Data [Occupation Number (ON), Their Orbital Energy *E* (in au), Second-Order Perturbation Energy (Donor → Acceptor) (in kcal/mol), and Wiberg Bond Order] Calculated at B3LYP/6-31+G(d) Level of Theory for TS1b-aq and TS1c-aq[a]

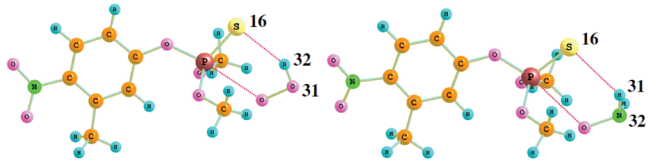

TS1b-aq TS1c-aq

species	ON (n1S16)	*E* (n1S16)	n1(S16) → σ*(P−Q)	Wiberg BO (S16−Q)
TS1b-aq	1.829	−0.218	8.46	0.0429
TS1c-aq	1.827	−0.215	3.38	0.0164

[a]P = O31, Q = H32 for **TS1b-aq** and P = N32, Q = H31 for **TS1c-aq**.

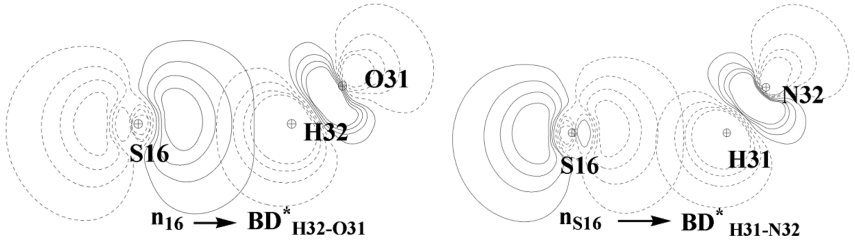

Figure 6. $n_S \rightarrow BD^*_{XH}$ (X = O, N) orbital overlap diagrams (contour) for **TS1b-aq** and **TS1c-aq**.

kcal/mol. The enthalpy of activation for **TS1b-aq** is 6.47 kcal/mol which is almost half of that of **TS1a-aq**. This observation indicates that the α-nucleophile, OOH^-, is very much more reactive than the simple nucleophile, OH^-. This can be explained by the stability of the corresponding transition state which is stabilized by the intermolecular H-bond between the peroxide hydrogen and the sulfur atom of **FN**. In case of **TS1b-aq**, the interaction is stronger than that of **TS1a-aq**, as the hydrogen-bond distance (S···H) of **TS1b-aq** is 0.51 Å less than that of **TS1a-aq**. The aforementioned observation clearly leads to the conclusion that hydroperoxidolysis is much faster than hydrolysis of **FN**.

*3.1.3. Reaction of **FN** with Hydroxylamine Anion (NH_2O^-).* Hydroxylamine anion is also an efficient α-nucleophile for the detoxification of **FN** and other organophosphate esters. Hydroxylamine, an oxygen nucleophile, reacts with **FN** through anionic oxygen at high pH, though depending on pH it can exist in three different protonation forms.[69−71] The B3LYP/6-31+G(d) free energy diagrams for the reaction path for both gas-phase and aqueous-phase solvolysis of **FN** with NH_2O^- are presented in Figure 5.

The concerted S_N2 reaction scheme for the gas phase is depicted in Figure 2 (channel c), and the coordinates of gas-phase optimized geometries are presented in the Supporting Information. This nucleophilic reaction follows the similar mechanisms presented above for the OH^- and OOH^- α-nucleophiles, and the initial nucleophilic attack resulted in an exergonic adduct (**RCc**) with 23.54 kcal/mol. In **RCc**, the P−OAr and P−ONH_2 distances are 1.62 and 3.84 Å, respectively. The hydrogen bond between the oxygen of the nucleophile and the H of the $-OCH_3$ of **FN** has a interaction distance of 1.99 Å. Also, it is worth mentioning here that the nucleophile possesses a symmetric arrangement with respected to the two $-OCH_3$ groups of **FN**. The **RCc** once formed transforms into the more stable product complex, **PCc**, through a TBP geometric transition state, **TS1c**, with activation barrier, 4.03 kcal/mol. From **RCc** to **TS1c**, the active distances, P−OAr and P−ONH_2, change from 1.62 to 1.68 and 3.84 to 3.04 Å, respectively. In the final product, **PCc**, a symmetry inversion occurs at the P center and **PCc** lies 63.2 kcal/mol below the separated reactants (**FN** + NH_2O^-). In the product complex, **PCc**, the P−OAr and P−ONH_2 distances are 4.56 and 1.65 Å, respectively. These distances are 2.88 Å larger and 1.39 Å shorter than the corresponding distances in the transition state, **TS1c**.

The B3LYP/6-31+G(d) optimized geometries for aqueous-phase solvolysis of **FN** are shown in Figure 1. The aqueous-phase reaction of **FN** with NH_2O^- goes directly through the transition state, **TS1c-aq**, with the activation free energy of 19.68 kcal/mol and the activation enthalpy of 7.42 kcal/mol. As seen from Table 1, the **TS1c-aq** possesses a slightly higher barrier (1 kcal/mol for $\Delta G^{\ddagger}$ and 0.86 kcal/mol for $\Delta H^{\ddagger}$) than **TS1b-aq**. The **TS1c-aq** can also be considered as an early transition state and has TBP geometry in which the P−OAr and P−ONH_2 distances are 1.69 and 2.77 Å, respectively. The distance between the S atom and closer H atom of the nucleophile that determines the H-bond strength is 2.67 Å, which is 0.30 Å longer than that in **TS1b-aq**.

According to our findings, **TS1c-aq** possesses a nearly similar activation barrier compared to **TS1b-aq**, which is an apparent conflict between the experimental results and our theoretical findings. In early research in this field, it was observed that the reactivity of OOH^- is 2.46 times greater than NH_2O^-.[15] This may be due to the limitations of theoretical methods to incorporate all the experimental conditions.

3.2. Reactivity of Two α-Nucleophiles. Following the above discussion the relative reactivity of two α-nucleophiles needs special attention. We have evaluated some important conceptual parameters related to nucleophilic reactivity to establish OOH^- as a stronger nucleophile than NH_2O^- for the S_N2@P reaction of **FN**. The approaches considered here for comparison of reactivity of the α-nucleophiles were successfully applied by Kesharwani et al.[16]

dx.doi.org/10.1021/jp2100057 | J. Phys. Chem. A 2012, 116, 2536−2546

The most important factor that favors the hydroperoxidolysis over the solvolysis by the hydroxylamine is the strength of intermolecular H-bonding in the corresponding transition states, **TS1b-aq** and **TS1c-aq**. To quantify the strength of intermolecular H-bonding, NBO analysis is performed on the transition states, **TS1b-aq** and **TS1c-aq**. The occupation number (ON) and significant donor−acceptor interactions measured by second-order perturbation energies, tabulated in Table 2, are obtained from NBO analysis.

The second-order perturbation energies for the interaction of the lone pair of the donor S16 (n1S16) and acceptor σ^* (O31−H32 for **TS1b-aq** and N32−H31 for **TS1c-aq**) are 8.86 and 3.38 kcal/mol, respectively, which suggest that such interaction is stronger in the case of **TS1b-aq**. The comparison of interaction is shown in the contour plot for orbital overlap depicted in Figure 6.

The Wiberg bond order for the intermolecular H-bond in the respective TS shows that the H-bond in **TS1b-aq** is almost 3 times stronger than that in **TS1c-aq** (refer to Table 2).

As a second strategy, the theory of AIM has been applied to define and describe the H-bonding phenomena in the transition states formed by the attack of two α-nucleophiles with **FN** in the aqueous phase. The necessary indicator for the existence of Y···X (S···H) interaction is the presence of a bond (3, −1) type critical point (CP) (in which curvature of the density at the CP along the line connecting two nuclei is positive and the two curvatures along mutually perpendicular lines and perpendicular to the bond path are negative) on which other topological properties such as the electron density (ρBCP) gradient and Laplacian of the electron density ($\nabla^2\rho$BCP) are calculated for characterizing the nature and strength of the Y···X interaction.[51] The calculated AIM parameters are presented in Table 3.

According to Popelier and Bader there exists a standard condition for H-bonding in AIM formalism.[72] The extent of electron density, ρBCP, and its Laplacian, $\nabla^2\rho$BCP, for a normal H-bond at the CP should occur in between 0.002 and 0.035 and 0.024 and 0.139 au,[73] respectively. From the values in Table 3 it can clearly be found that the ρBCP (0.0203 and 0.0121) and $\nabla^2\rho$BCP (0.05544 and 0.03866) are within the range mentioned above, and consequently the existence of H-bonding interaction is strongly confirmed. The topological analysis further suggests that the intermolecular H-bonding interaction in **TS1b-aq** is much stronger than that in **TS1c-aq**, which supports the NBO outcomes as well.

Table 3. B3LYP/6-31+G(d) Calculated Electron Density (ρ) and Laplacian of the Electron Density ($\nabla^2\rho$) at the Bond Critical Point (BCP) in au for H-Bonds

species	bond (P−Q)	ρ	$\nabla^2\rho$
TS1b-aq	S16−H32	0.0203	0.05544
TS1c-aq	S16−H31	0.0121	0.03866

One straight-forward approach considered here is to find out the difference between the relative magnitudes of above-mentioned H-bonding interactions in the transition states. Howard[74] proposed an idea to estimate the strength of a H-bond using a vibrationless model and its components at infinite separation of the molecular system. In this notion, the energies of **FN** and nucleophiles are calculated separately using the structure derived from respective transition state without perturbing the geometry. Finally, the energy difference between separated molecules and the TS is considered as the H-bond strength. From the energy difference calculated at MP2/6-311++G(2d,2p) level of theory, it is found that the H-bond in **TS1b-aq** is 1.79 kcal/mol stronger than that in **TS1c-aq** (presented in Figure S2 in the Supporting Information).

Furthermore, a conceptual DFT analysis (by means of electron density as the fundamental property) is performed to obtain the order of reactivity of α-nucleophile with **FN**. The difference of local softness of nucleophile and electrophile is calculated and analyzed according to the HSAB principle. The complete procedure of calculation has already been described in the Computational Procedures section of this article. The calculated Fukui function (f) and local softness parameters (s^+ and s^-) are presented in Table 4, and the differences (Δs) of s^+ and s^- are given in Table 5.

Table 5. Reactivity in the Gas Phase and Aqueous Phase as Measured by the Difference in Local Softness (Δs) for Fenitrothion and α-Nucleophiles (HOO^- and NH_2O^-) using Different Charge Analyses

	Δs		
species	NPA	Mulliken	Chelpg
HOO^-	3.961 (3.239)	4.334 (3.395)	4.769 (3.644)
NH_2O^-	5.294 (3.294)	5.443 (3.432)	5.566 (3.432)

The Δs values are lower for OOH^-, and these are entirely consistent for three different types of charge analysis, NPA, Mulliken, and Chelpg. It is noteworthy to mention here that Δs for two different nucleophiles shows a similar trend in both gas and aqueous phases. Therefore, the conceptual DFT results clearly infer that the reactivity of OOH^- is always greater than that of NH_2O^- for the S_N2@P attack on **FN**, which strongly supports the previously reported NBO and AIM conclusions.

Finally, from the above analysis the reactivity trends for simple as well as α-nucleophiles for the S_N2@P reactions with **FN** have been undoubtedly established. Therefore, the order of reactivity is predicted to be $OOH^- > NH_2O^- \gg OH^-$, which correlates well with the experimental findings.

Table 4. Global Softness (S), Local Softness (s^+), and Fukui Function (f) for the α-Nucleophiles (HOO^- and NH_2O^-) and Fenitrothion Calculated using NPA, Mulliken, and Chelpg Charges at B3LYP/6-31+G(d) Level in the Gas as Well as in the Aqueous Phase (in Parentheses)

		f			s^+ and s^-		
species	S	NPA	Mulliken	Chelpg	NPA	Mulliken	Chelpg
HOO^-	5.655 (4.603)	−0.686 (−0.698)	−0.694 (−0.711)	−0.653 (−0.685)	−3.879 (−3.213)	−3.924 (−3.272)	−3.692 (−3.153)
NH_2O^-	8.118 (5.036)	−0.642 (−0.649)	−0.62 (−0.657)	−0.553 (−0.584)	−5.212 (−3.268)	−5.033 (−3.309)	−4.489 (−2.941)
FN	6.297 (6.501)	0.013 (0.004)	0.065 (0.019)	0.171 (0.057)	0.081 (0.0260)	0.409 (0.123)	1.076 (0.4908)

dx.doi.org/10.1021/jp2100057 | J. Phys. Chem. A 2012, 116, 2536−2546

3.3. S_N2@C Reactions. The S_N2@C reactions with three nucleophiles have been studied in the aqueous phase only. The necessary optimized geometries at B3LYP/6-31+G(d) level of theory in the aqueous phase are presented in Figure 1. **FN** has two aliphatic methyl groups connected with the central P atom through the O atom. The spatial orientations of two methyl groups are anti to each other, and with respect to the phosphorus atom they are nearly identical, as the angle P−O−C and the P−O bond length are almost the same. Consequently, two pathways have been investigated for the S_N2@C reaction for each nucleophile. The lower energetic pathway is described here in detail. A combined free energy (ΔG_{298k}) profile obtained at B3LYP/6-31+G(d) level for the S_N2@C reactions with three different nucleophiles in the aqueous phase is presented in Figure 7.

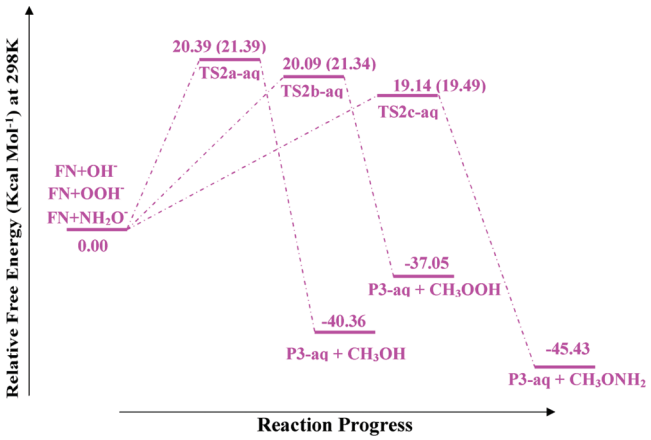

Figure 7. B3LYP/6-31+G(d) calculated free energy (ΔG_{298k}) profile for the reaction of fenitrothion with nucleophiles at the aliphatic carbon center (S_N2@C) in the aqueous phase.

3.3.1. Reaction with OH^-. Similar to the S_N2@P reactions in the aqueous phase, in the S_N2@C reaction the separated reactants go directly to the transition state, **TS2a-aq**, with activation barrier of 20.39 kcal/mol. It also possesses activation enthalpy of 12.16 kcal/mol. The nucleophile, OH^-, attacks at the C center through the backside of the leaving group and produces a perfectly TBP geometry for TS. In TS, the bond-forming and bond-breaking distances (C−O) are 2.19 and 1.79 Å, respectively, and the corresponding O−C−O angle is 177.3°. The resulting reaction is highly exergonic by 40.36 kcal/mol.

3.3.2. Reaction with OOH^-. The OOH^- also attacks the C center of **FN** from the backside of the leaving group in the same way as the OH^- does and produces a TBP geometric transition state, **TS2b-aq**, that possesses Gibbs energy of activation of 20.09 kcal/mol and enthalpy of activation of 10.35 kcal/mol. In the transition state, the bond-forming and bond-breaking distances are 2.16 and 1.77 Å, respectively, and the O−C−O angle is 175.9°. The activation barrier clearly suggests that the reactivity of the OOH^- is greater than that of the OH^- for the S_N2@C reactions of **FN**. This reaction is found to be slightly less exergonic than OH^-, and here the net difference in free energy is 42.32 kcal/mol.

3.3.3. Reaction with NH_2O^-. Like the previous two nucleophiles, NH_2O^- also attacks the aliphatic C center of **FN** in a concerted asynchronous S_N2 pathway through a TBP structural transition state, **TS2c-aq**. The resulting reaction is highly exergonic by 45.43 kcal/mol, which is the highest among the three nucleophiles. In **TS2c-aq**, the significant bond-forming and bond-breaking distances are 2.20 and 1.74 Å, respectively, and the angle of O−C−O is 176.4°. The **TS2c-aq** possesses an activation free energy of 19.14 kcal/mol and activation enthalpy of 9.07 kcal/mol. The free energy of activation of **TS2c-aq** is 0.95 and 1.25 kcal/mol lower than that for OOH^- and OH^-, respectively. Also, the enthalpy of activation of **TS2c-aq** is 1.29 and 3.09 kcal/mol lower than that for OOH^- and OH^-, respectively. Consequently, the order of reactivity for the S_N2@C pathways can be easily predicted from the energetics data, and it should be $NH_2O^- > OOH^- > OH^-$. This order of reactivity is also well-harmonized with the experimentally observed one.

After summarization of the results it is important to mention here that the orders of reactivity of OOH^- and NH_2O^- are altered with changing the reaction center of **FN**, i.e., from the S_N2@P to the S_N2@C. To get more insight into this interesting phenomenon of the reactivity, nucleophilic charge analysis is performed on the reactive centers of the two α-nucleophiles, and the results show that the nucleophilic oxygen of NH_2O^- bears a larger negative charge. Therefore, one can infer that NH_2O^- exhibits stronger nucleophilic nature than OOH^-. So the most plausible explanation for the above fact is that the S_N2@P reaction is controlled by the stabilization of the transition state as well as a steric effect which make the solvolysis process easier for OOH^- than NH_2O^-. On the other hand, the controlling factor for the S_N2@C reaction is nucleophilicity, which alters the reactivity trend.

4. CONCLUSION

The nucleophilic reactions of a variety of oxygen nucleophiles (simple and α-nucleophile) at the P and C centers of **FN** in vacuum and in water have been investigated in detail. This study also devotes to predict the trends of reactivity of the nucleophiles. The simple OH^- and α-nucleophiles, OOH^- and NH_2O^-, are considered here for a series of reactions of **FN** at the P and aliphatic C centers. The S_NAr pathway is not studied here as it has no experimental findings. Our computed data show that all the S_N2 reactions are occurred in a single-step concerted asynchronous pathway connected through a trigonal bipyramidal S_N2-like transition state, and at the product a complete inversion of stereochemistry of the attacking site is observed. The S_N2@P pathways are the most energetically favorable and consequently are the most important ones for the solvolysis of **FN** for all the nucleophiles. This is in accordance with the HSAB theory. All the nucleophiles examined here are "hard" O-nucleophiles, and they must have greater reactive tendency toward the "hard" P center than the "soft" electrophilic aliphatic carbon center. It is observed that the aqueous-phase reaction is energetically more favorable than the gas-phase one for all the nucleophiles investigated here. For the S_N2@P reactions, the relative reactivity of the nucleophiles is predicted to be $OOH^- > NH_2O^- > OH^-$ with reaction barriers of 18.68, 19.68, and 20.52 kcal/mol, respectively, in the aqueous phase indicating an important α-effect. The α-nucleophile OOH^- is found to be the most reactive for the reaction at the P center in **FN**. The NBO and AIM results show that the intermolecular H-bonding is very important to favor the reactions for OOH^-. The conceptual DFT analysis also confirms the above trend of reactivity. Concerning the relative magnitudes of the activation barriers determined for the S_N2@C reactions with different nucleophiles, it is observed that for the S_N2@C reactions the reactivity order gets altered from the

dx.doi.org/10.1021/jp2100057 | J. Phys. Chem. A 2012, 116, 2536−2546

S_N2@P and shows the trend NH_2O^- (19.14 kcal/mol) > OOH^- (20.09 kcal/mol) > OH^- (20.39 kcal/mol). For NH_2O^-, the main pathway is the S_N2@P, whereas in the case of S_N2@C reaction it possesses the lowest activation barrier than the other two. The overall results are in excellent agreement with experimental observations.

■ ASSOCIATED CONTENT

Supporting Information

The conformational analysis, relative energy of the conformers, Cartesian coordinates for optimized geometries in gas and aqueous phases for all the species, ZPVE, thermochemical parameters, imaginary frequencies of the transition states, and calculation of H-bond strength. This material is available free of charge via the Internet at http://pubs.acs.org.

■ AUTHOR INFORMATION

Corresponding Author

*E-mail: spakd@iacs.res.in.

Present Address

[†]WestChem, Department of Pure and Applied Chemistry, University of Strathclyde, Glasgow, U.K.

Notes

The authors declare no competing financial interest.

■ ACKNOWLEDGMENTS

We are grateful to the reviewer for valuable comments and suggestions to improve the manuscript. D.M. is very much grateful to the Council of Scientific and Industrial Research (CSIR), Government of India, for providing a Junior Research Fellowship. We thank Ms. D. Ghosh and Mr. S. Bagchi for helpful discussions.

■ REFERENCES

(1) *Chemistry and World Food Supplies: The New Frontiers—CHEMRAWN II*; Bixler, G., Shemilt, L. W., Eds.; IUPAC/IRRI: Manila, Philippines, 1983.
(2) Wan, H. B.; Wong, M. K.; Mok, C. Y. *Pestic. Sci.* **1994**, *42*, 93−99.
(3) Ohshiro, K.; Kakuta, T.; Sakai, T.; Hirota, H.; Hoshino, T.; Uchiyama, T. *J. Ferment. Bioeng.* **1996**, *82*, 299−305.
(4) Lartiges, S. B.; Garrigues, P. P. *Environ. Sci. Technol.* **1995**, *29*, 1246−1254.
(5) Lacorte, S.; Barcelo, D. *Environ. Sci. Technol.* **1994**, *28*, 1159−1163.
(6) Durand, G.; Mansour, M.; Barcelo, D. *Anal. Chim. Acta* **1992**, *262*, 167−178.
(7) Liu, B.; McConnell, L. L.; Torrents, A. *Chemosphere* **2001**, *44*, 1315−1323.
(8) Macalady, D. L.; Wolfe, N. L. *J. Agric. Food Chem.* **1983**, *31*, 1139−1147.
(9) Maguire, R. J.; Hale, E. J. *J. Agric. Food Chem.* **1980**, *28*, 372−378.
(10) Wolfe, N. L.; Zepp, R. G.; Gordon, J. A.; Baughman, G. L.; Cline, D. M. *Environ. Sci. Technol.* **1977**, *11*, 88−93.
(11) Bavcon, K. M.; Franco, M.; Trebse, P. *Chemosphere* **2007**, *67*, 99−107.
(12) Wanner, O.; Egli, T.; Fleischman, T.; Lanz, K.; Reichert, P.; Schwarzenbach, R. P. *Environ. Sci. Technol.* **1989**, *23*, 1232−1242.
(13) Han, X.; Balakrishnan, V. K.; vanLoon, G. W.; Buncel, E. *Langmuir* **2006**, *22*, 9009−9017.
(14) Omakor, J. E.; Onyido, I.; vanLoon, G. W.; Buncel, E. *J. Chem. Soc., Perkin Trans.* **2001**, *2*, 324−330.
(15) Rougier, N. M.; Vico, R. V.; Rossi, R. H. D.; Bujan, E. I. *J. Org. Chem.* **2010**, *75*, 3427−3436.
(16) Kesharwani, M. K.; Khan, M. A. S.; Bandyopadhyay, T.; Ganguly, B. *Theor. Chem. Acc.* **2010**, *127*, 39−47.
(17) Mandal, D.; Mondal, B.; Das, A. K. *J. Phys. Chem. A* **2010**, *114*, 10717−10725.
(18) Kazimierowicz, E. D.; Sokalski, W. A.; Leszczynski, J. *J. Phys. Chem. B* **2008**, *112*, 9982−9991.
(19) Xiong, Y.; Zhan, C. G. *J. Org. Chem.* **2004**, *69*, 8451−8458.
(20) Patterson, E. V.; Cramer, C. G. *J. Phys. Org. Chem.* **1998**, *11*, 232−240.
(21) Greenhalgh, R.; Dhawan, K. L.; Weinberger, P. *J. Agric. Food Chem.* **1980**, *28*, 102−105.
(22) *Handbook of Organophosphorus Chemistry*; Engel, R., Ed.; Marcel Dekker: New York, 1992; pp 465−469.
(23) Mortland, M. M.; Raman, K. V. *J. Agric. Food Chem.* **1967**, *15*, 163−167.
(24) Blanchet, P. F.; St-George, A. *Pestic. Sci.* **1982**, *13*, 85−91.
(25) Dust, J. M.; Warren, C. S. *Water Qual. Res. J. Can.* **2001**, *36*, 589−604.
(26) Onyido, I.; Omakor, J. E.; van-Loon, G. W.; Buncel, E. *ARKIVOC* **2001**, *2*, 134−142.
(27) Smolen, J. M.; Stone, A. T. *Environ. Sci. Technol.* **1997**, *31*, 1664−1673.
(28) Koo, I. S.; Ali, D.; Yang, K.; vanLoon, G. W.; Buncel, E. *Bull. Korean Chem. Soc.* **2009**, *30*, 1257−1261.
(29) Balakrishnan, V. K.; Han, X.; vanLoon, G. W.; Dust, J. M.; Toullec, J.; Buncel, E. *Langmuir* **2004**, *20*, 6586−6593.
(30) Katagi, T. *J. Agric. Food Chem.* **1989**, *37*, 1124−1130.
(31) Choi, H.; Yang, K.; Park, J. K.; Koo, I. S. *Bull. Korean Chem. Soc.* **2010**, *31*, 1339−1342.
(32) Koo, I. S.; Ali, D.; Yang, K.; Park, Y.; Wardlaw, D. M.; Buncel, E. *Bull. Korean Chem. Soc.* **2008**, *29*, 2252−2258.
(33) Allouche, A. R. *Gabedit*. http://gabedit.sourceforge.net/.
(34) Stewart, J. J. P. MOPAC2009; Stewart Computational Chemistry, version 9.259W. http://openmopac.net/.
(35) Ali, S.;et al. Avogadro: an open-source molecular builder and visualization tool, version 1.0.3. http://avogadro.openmolecules.net/wiki/Main_Page/.
(36) Becke, A. D. *J. Chem. Phys.* **1993**, *98*, 5648−5662.
(37) Lee, C. T.; Yang, W. T.; Parr, R. G. *Phys. Rev. B* **1988**, *37*, 785−789.
(38) Miehlich, B.; Savin, A.; Stoll, H.; Preuss, H. *Chem. Phys. Lett.* **1989**, *157*, 200−206.
(39) Dill, J. D.; Pople, J. A. *J. Chem. Phys.* **1975**, *62*, 2921−2923.
(40) Gonzales, C.; Schlegel, H. B. *J. Chem. Phys.* **1989**, *90*, 2154−2162.
(41) Gonzales, C.; Schlegel, H. B. *J. Phys. Chem.* **1990**, *94*, 5523−5527.
(42) Møller, C.; Plesset, M. S. *Phys. Rev.* **1934**, *46*, 618−622.
(43) Head-Gordon, M.; Pople, J. A.; Frisch, M. J. *Chem. Phys. Lett.* **1988**, *153*, 503−506.
(44) Frisch, M. J.; Head-Gordon, M.; Pople, J. A. *Chem. Phys. Lett.* **1990**, *166*, 275−280.
(45) Frisch, M. J.; Head-Gordon, M.; Pople, J. A. *Chem. Phys. Lett.* **1990**, *166*, 281−289.
(46) Klamt, A.; Schuurmann, G. *J. Chem. Soc., Perkin Trans.* **1993**, *2*, 799−805.
(47) Frisch, M. J.;et al. *Gaussian 09*, revision B.01; Gaussian, Inc.: Pittsburgh, PA, 2009.
(48) Tomasi, J.; Persico, M. *Chem. Rev.* **1994**, *94*, 2027−2094.
(49) Cossi, M.; Barone, V.; Cammi, R.; Tomasi, J. *Chem. Phys. Lett.* **1996**, *255*, 327−335.
(50) Barone, V.; Cossi, M.; Tomasi, J. *J. Chem. Phys.* **1997**, *107*, 3210−3221.
(51) Barone, V.; Cossi, M.; Tomasi, J. *J. Comput. Chem.* **1998**, *19*, 404−417.
(52) Cossi, M.; Barone, V. *J. Chem. Phys.* **1998**, *109*, 6246−6254.
(53) Seckute, J.; Menke, J. L.; Emnett, R. J.; Patterson, E. V.; Cramer, C. J. *J. Org. Chem.* **2005**, *70*, 8649−8660.
(54) Bader, R. F. W. *Atoms in Molecules. A Quantum Theory*; Oxford University Press: New York, 1994.

(55) Cioslowski, J.; Nanayakkara, A.; Challacombe, M. *Chem. Phys. Lett.* **1993**, *203*, 137−142.
(56) Cioslowski, J. *Chem. Phys. Lett.* **1994**, *219*, 151−154.
(57) Biegler-Konig, F.; Schonbohm, J.; Bayles, D. AIM2000, A program to analyze and visualize atoms in molecules. *J. Comput. Chem.* **2001**, *22*, 545−559.
(58) Glendening, D. E.; Reed, A. E.; Carpenter, J. E.; Winhold, F. NBO, version 3.1, 1992.
(59) Yang, W.; Parr, R. G. *Proc. Natl. Acad. Sci. U.S.A.* **1985**, *82*, 6723−6726.
(60) Parr, R. G.; Yang, W. *J. Am. Chem. Soc.* **1984**, *106*, 4049−4050.
(61) Yang, W.; Mortier, W. J. *J. Am. Chem. Soc.* **1986**, *108*, 5708−5711.
(62) Reed, A. E.; Curtiss, L. A.; Weinhold, F. *Chem. Rev.* **1988**, *88*, 899−926.
(63) Mulliken, R. *J. Chem. Phys.* **1955**, *23*, 1833−1841.
(64) Breneman, C.; Wiberg, K. *J. Comput. Chem.* **1990**, *11*, 361−373.
(65) Koopmans, T. A. *Physica* **1934**, *1*, 104−113.
(66) Gazquez, J. L. *J. Phys. Chem. A* **1997**, *101*, 4657−4659.
(67) Nguyen, L. T.; Le, T. N.; Proft, F. D.; Chandra, A. K.; Lengenaeker, W.; Nguyen, M. T.; Geerlingl, P. *J. Am. Chem. Soc.* **1999**, *121*, 5992−6001.
(68) Ponti, A. *J. Phys. Chem. A* **2000**, *104*, 8843−8846.
(69) Kirby, A. J.; Manfredi, A. M.; Souza, B. S.; Medeiros, M.; Priebe, J. P.; Brandao, T. A. S.; Nome, F. *ARKIVOC(III)* **2009**, 28−38.
(70) Kirby, A. J.; Souza, B. S.; Medeiros, M.; Priebe, J. P.; Manfredi, A. M.; Nome, F. *Chem. Commun.* **2008**, 4428−4429.
(71) Kirby, A. J.; Davies, J. E.; Brandao, T. A. S.; da Silva, P. F.; Rocha, W. R.; Nome, F. *J. Am. Chem. Soc.* **2006**, *128*, 12374−12375.
(72) Popelier, P. L. A.; Bader, R. F. W. *Chem. Phys. Lett.* **1992**, *189*, 542−548.
(73) Nowroozi, A.; Jalbout, A. F.; Roohi, H.; Khalilinia, E.; Sadeghi, M.; Leon, A. D.; Raissi, H. *Int. J. Quantum Chem.* **2009**, *109*, 1505−1514.
(74) Howard, S. T. *J. Am. Chem. Soc.* **2000**, *122*, 8238−8244.